Crystal Structure Prediction of Energetic Materials

Joseph E. Arnold and Graeme M. Day*

School of Chemistry, University of Southampton, Southampton, SO17 IBJ, UK

E-mail: G.M.Day@soton.ac.uk

Abstract

The synthesis and experimental testing of energetic materials can be hazardous, but their many industrial and military applications necessitate their constant research and development. We evaluate computational methods for predicting the crystal structures of energetic molecular organic crystals from their molecular structure as a first step in computationally evaluating materials, which could guide experimental work. Crystal structure prediction (CSP) is evaluated on a test set of ten energetic materials with known crystal structures, initially using a rigid-molecule, anisotropic atom-atom force field approach, followed by re-optimization of predicted crystal structures using dispersion-corrected solid state density functional theory (DFT). CSP using the force field was found to provide good results for some molecules, whose known crystal structures are reproduced by one of the lowest energy predictions, but are more variable than for other small organic molecules. Re-optimization of predicted crystal structures using solid state DFT leads to reliable predictions, demonstrating CSP as an approach that can be applied in the area of energetic materials discovery and development.

Introduction

Energetic materials (EMs) are a class of compounds which, upon initiation, for example, by mechanical impact or heat, release a large amount of stored chemical energy. The development of new energetic materials is critical as EMs are a vital component of many industrial processes (e.g. mining and aero-space industries) as well as their many uses in the defence sector (e.g. propellants and explosives).[1–9] However, the inherent dangers with synthesizing, handling and testing EMs presents a clear opportunity to develop computational methods to predict the structure and properties of new materials in advance of their synthesis, thus minimizing unnecessary experimentation.

Inherent molecular properties are clearly important in the design of EMs, but the mutual arrangement of molecules in the material dictates how energy is transferred, and in turn also dictates important properties such as impact sensitivity and detonation velocity: this is evident from property variation between polymorphs of some EMs.[10] Therefore, computational approaches for guiding the development of EMs should include the prediction of how EM molecules are arranged in the solid state.

Crystal structure prediction (CSP) aims to predict all possible polymorphs for a compound given only its molecular structure.[11,12] This is usually approached through a computational exploration of the lattice energy surface to identify all low energy local minima, which correspond to putative stable crystal packings of the molecule being studied. The structures associated with each local energy minimum are ranked according to their predicted energy, with the assumption that the most likely observable crystal structure corresponds to the lowest energy predicted structure - the global energy minimum. The two greatest challenges in CSP are the high dimensionality of the relevant energy surface, which creates a challenge in locating all possible crystal structures, and the small energies that typically separate competing predicted crystal structures. The energy differences between predicted crystal structures are often of the order of 1 kJ mol^{-1} or less, meaning that high quality models are required for evaluating the relative energies of predicted crystal structures; the errors in

force field[13] and electronic structure methods[14–16] for lattice energies are often larger than these energy differences and so partly rely on cancellation of errors when evaluating relative energies.

CSP can be applied prior to synthesis; hypothetical molecules can be assessed via CSP to decide whether they are worth synthesizing. For known molecules, CSP can help anticipate polymorphism, beyond what has been experimentally observed to-date. Thus, a CSP landscape is a powerful tool for anticipating the crystal structures of as-yet unsynthesized molecules and predicting possible polymorphic forms of known molecules. The field has seen rapid development in methods used for structural exploration and energy ranking, such that CSP has been succesfully applied in a range of applications, such as polymorph screening of active pharmaceutical ingredients,[17,18] discovery of photocatalysts[19] and porous materials.[20]

The present work aims to assess the performance of CSP for molecular organic EMs. Previous studies have demonstrated successful CSP methodologies for individual systems; for example, Bier *et al.* demonstrated a successful CSP methdology using a genetic algoritm for structure generation combined with solid state density functional theory (DFT) energy ranking which reproduced the known crystal structures of 2,4,6-trinitrobenzene-1,3,5-triamine (TATB) and 2,4,6-trinitrobenzene-1,3-diamine (DATB).[21] Here, we validate the performance of a quasi-random structure search combined with an anisotropic atom-atom force field, as well as DFT reranking, for CSP on a broader set of ten EMs to assess the general applicability of CSP in the area of EMs. We also evaluate the sensitivity of force field predictions to the parameter set and electronic structure calculation from which electrostatics are derived.

Methods

CSP

Ten known EMs, all with experimentally determined crystal structures, were chosen for validation of CSP methods. The test set of EMs studied is shown in Figure 1.[22–38] Some of the

validation molecules are known to exhibit polymorphism; the number of known polymorphs for each molecule is shown in parentheses in Figure 1.

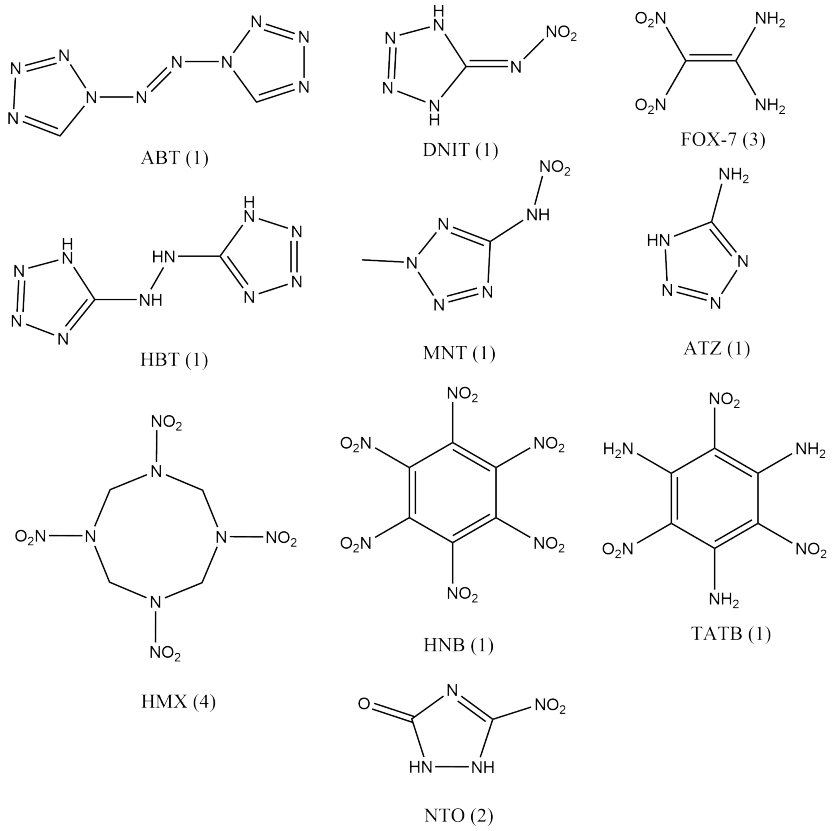

Figure 1: The molecular diagrams of 1,1'-azobistetrazole (ABT), 4,5-dihydro-5-nitrimino-1H-tetrazole (DNIT), hexanitrobenzene (HNB), 2-methyl-5-nitramino-2H-tetrazole (MNT), 1,3,5,7-tetranitro-1,3,5,7-tetrazocane (HMX), 1,1-diamino-2,2-dinitroethene (FOX-7), 5,5'-hydrazinebistetrazole (HBT), nitrotriazolone (NTO), 2,4,6-triamino-1,3,5-trinitrobenzene (TATB) and 5-amino-1H-tetrazole (ATZ). The number in parentheses represents the number of known polymorphs for each EM.

CSP was performed using the Global Lattice Energy Explorer (GLEE) package,[39] which uses a low-discrepancy, quasi-random sampling of crystal packing variables to explore the lattice energy surface, followed by rigid-molecule lattice energy minimization using an intermolecular force field (described below). Molecular geometries of each molecule were optimized using DFT (PBE0/aug-cc-pVDZ, using Gaussian[40]) starting from the conformations in their observed crystal structures. The test set contains mostly rigid molecules, so a rigid-molecule approach was taken for generating predicted crystal structures using the gas phase

optimized minimum of each EM. Low energy predicted crystal structures were re-optimized using solid state DFT to account for molecular distortion due to intermolecular interactions in the crystal structures. We analyze the impact of DFT re-optimization on the quality of the predictions.

HMX was the only EM in the set with more than one conformer present within the known polymorphs. The conformations differ in the geometry of the eight-membered ring and are sometimes referred to as chair (β, ϵ polymorphs) and chair-chair (α, δ) in discussions of HMX polymorphism.[41] For HMX, CSP was performed on the chair and chair-chair conformers, both of which were optimized as described above. In the force field evaluation studies, these CSPs were treated separately due to the large conformational energy difference which exists between the two conformers of HMX. For the force field results, we compare total relative energies, calculated from the sum of intermolecular energies and relative conformational energies as in Equation 1.

$$E_{latt} = U_{inter} + \Delta E_{intra} \tag{1}$$

where U_{inter} is the intermolecular contribution to the lattice energy calculated using the force field, and ΔE_{intra} is the DFT energy of the molecular geometry in the crystal, relative to the lowest energy conformer.

DMACRYS was used with an anisotropic atom-atom force field energy model for all lattice energy minimizations.[42] To test the sensitivity of CSP results to the force field, CSP was performed using two commonly used interatomic potentials (FIT[43] and W99rev[44]), combined with four combinations of generation methods for the electrostatic model: B3LYP[45,46] with 6-31G**,[47] 6-311G**,[48] 6-31G** with the polarizable continuum model (PCM[49]) and 6-311G** with the PCM applied. The PCM is used to mimic the in-crystal environment of a molecule. This provides a efficient, but approximate model of polarization contributions to the overall lattice energy.[50]

Distributed Multipole Analysis (DMA)[51] has been used to provide a description of the

intermolecular electrostatic interactions. Atomic multipoles, up to hexadecapole, were calculated using the Gaussian Distributed Multipole Analysis (GDMA) program,[52] which analyses the charge density calculated for the gas phase molecular geometry to produce the multipoles. Each EM in the test set was examined with the following combinations of methods for the electrostatic model: HF,[53] MP2,[54] PBE,[55,56] PBE0[57] and B3LYP[45,46] all with aug-cc-pVDZ and aug-cc-pVTZ.[58–60] The aforementioned results with B3LYP and 6-31G** and 6-311G** are also included.

Trial crystal structures were generated for each EM and each combination of electrostatic model and force field. The trial structures were then lattice energy minimized until a total of 20,000 successfully optimized structures were generated in each space group for each CSP. Crystal structures were generated with one molecule in the asymmetric unit cell (Z' = 1) for each combination of EM, force field and electrostatic model. These structures were produced by sampling in the 10 most frequently observed space groups for organic molecular crystals[61] ($P\bar{1}, P2_1, C2, Cc, P2_1/c, C2/c, P2_12_12_1, Pca2_1, Pna2_1, Pbca$).

Duplicates were removed from the resulting set of structures within each space group by calculating the similarity of simulated powder X-ray diffraction patterns obtained via the PLATON package[62] and comparing these using constrained dynamic time warping. Duplicate removal was performed with tight tolerances and was not performed between space groups at this stage. This was to prevent removal of structures that could lead to separate minima during the DFT re-optimization stage (described below).

To analyse the success of each CSP, the predicted structures were compared to experimental structures using the COMPACK algorithm.[63,64] COMPACK searches were carried out by comparing intermolecular atom-atom distances within a cluster of 30 molecules with 30% distance tolerances and 30° angle tolerances and a root mean squared deviation in atomic positions ($RMSD_{30}$) was calculated for the overlay of predicted and experimental structures.

Periodic DFT Re-Optimization

For all 10 EMs, the CSP set of crystal structures generated with the PBE0/aug-cc-pVTZ multipole model was further optimized using plane-wave-based periodic DFT as implemented in the VASP package.[65,66] For each EM, all structures on the respective CSP landscape within 10 kJ mol^{-1} of the global energy minimum were re-optimized. For ATZ, the energy window was increased to within 12 kJ mol^{-1} of the global energy minimum due to finding the experimental match just below 12 kJ mol^{-1}. This re-optimization was performed in a three-step procedure that has been found to improve the convergence rate of periodic DFT optimizations for crystal structures.[67] The first step involves optimizing only the atomic positions with the unit cell fixed, the second step optimizes both atomic positions and unit-cell parameters, and the third step is a final single-point calculation which updates the plane wave basis set to the newly relaxed lattice parameters to provide an accurate final energy. All VASP calculations were performed using the PBE exchange correlation function with the GD3BJ dispersion correction.[68] The projector augmented wave method was used for all VASP calculations with the standard supplied pseudopotentials.[69] Following this optimization, a more stringent removal of duplicates was carried out by using the COMPACK algorithm for all structures within 10 kJ mol^{-1} of the global energy minimum for each CSP, irrespective of the space group of each structure.[63]

Results and discussion

CSP is relatively under-explored for EMs. Because of this, we present an evaluation of the performance of different commonly used force fields and electrostatic models for CSP. The force field we use combines an empirically parameterized repulsion-dispersion model with an electrostatic model using atomic multipoles derived from a calculated electron density. Certain structures are very sensitive to the electrostatic model used for CSP. We have found that structures with high nitrogen content can be more sensitive to the electrostatic model

than those without.[70] Our initial CSPs on NTO, ATZ and TATB produced landscapes of varying quality using a typical electrostatic model; the $RMSD_{30}$ values (RMSD of atomic positions in a finite cluster of 30 molecules taken from the two crystal structures being compared) of the matches to the experimental structures covered a range from 0.186 Å to 1.004 Å. Figure 2 displays this $RMSD_{30}$ range via an overlay of the matched predicted crystal structure to the experimental structure for NTO and TATB; the structure of the β polymorph of NTO is reproduced poorly ($RMSD_{30}$ = 1.004 Å), while the known structure of TATB is reproduced accurately ($RMSD_{30}$ = 0.186 Å).

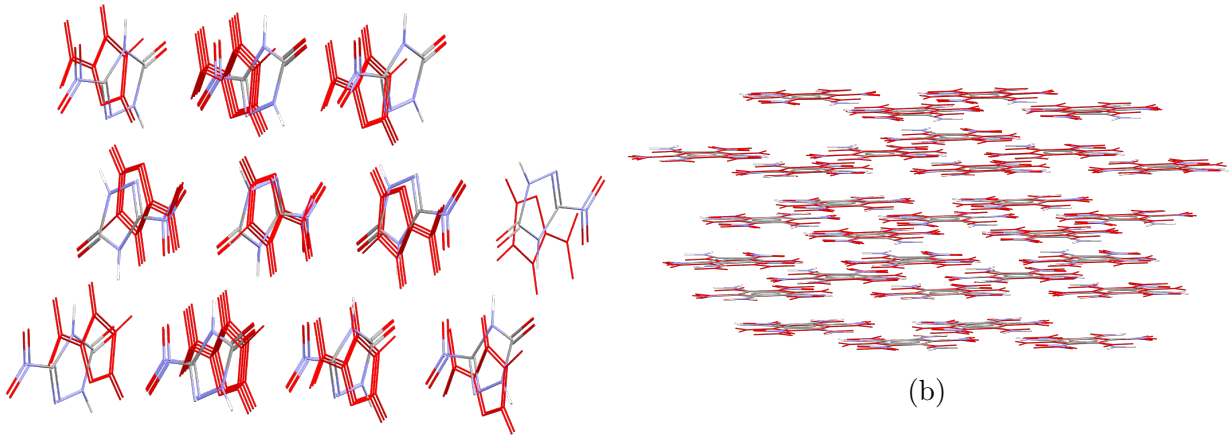

(a) (b)

Figure 2: Visualization of the $COMPACK_{30}$ comparison for the predicted crystal structure matches to the experimental structure for the initial CSP of β - NTO and TATB. These calculations used the FIT force field with multipoles derived from a B3LYP/6-311G** charge density. The experimental structures are shown with colouring by element and the predicted matches are shown in full red colouring. (a) Overlay of the matched predicted crystal structure to the experimental structure of NTO with $RMSD_{30}$ = 1.004 Å. (b) Overlay of the matched predicted crystal structure to the experimental structure of TATB with $RMSD_{30}$ = 0.186 Å.

The range in how well the known crystal structures were reproduced encouraged us to examine how optimizing the electrostatic model could improve the quality of the CSPs. The choice of force field, between FIT[43] and revised version of the Williams99 exp-6 potential[44] (W99rev), was also examined.

Choice of Force Field

FIT and W99rev are two force fields that are commonly used in modelling molecular organic crystals.[39,43,44] Both of these force fields are parameterized against structural and energetic information from known crystal structures, and were developed to function in tandem with anisotropic atomic multipole electrostatics. Using atomic multipoles has clear benefits over using isotropic point changes: they result in a more accurate electrostatic model due to the difference in the quality of the representation of electrostatic features such as π - electron density and lone pairs,[71] which leads to improved performance of structure prediction.[72] The revised version of W99 has been parameterized for use with multipole electrostatics derived from a specific set of combinations of DFT functionals and basis sets: B3LYP/6-31G** and B3LYP/6-311G**. Both of these electrostatic models also have a variant that has been derived from the charge density calculated using a Polarizable Continuum Model (PCM).[49] Applying PCM to the electrostatic model can be used as an approximate treatment of molecular polarization in crystal structure modelling.[50]

As discussed, our initial CSPs on ATZ and NTO proved unsatisfactory; the closest predicted match to the experimental structure for both EMs possessed a high relative energy and large geometric deviations. Thus, our testing for the choices of force field and electrostatic model involved performing CSPs on the 10 molecules shown in Figure 1 for Z' = 1 structures. Results for eight out of the ten molecules are summarized in Figure 4; ATZ and α-FOX7 are not included in this initial evaluation of force fields because we found that flexibility of the NH_2 groups has an important impact on the results for these crystal structures. Full CSP data tables for these box plots can be found in the supplementary information. Figure 3 shows an example CSP result for 2-methyl-5-nitramino-2H-tetrazole (MNT), where a predicted structure matching the experimentally determined structure is identified as the second lowest energy structure (Figure 3a) and the structure reproduces the experimentally determined crystal structure accurately ($RMSD_{30}$ = 0.190 Å, Figure 3b). To evaluate the force fields, we examined how well they reproduced the experimentally determined crystal

structures by measuring the $RMSD_{30}$ between the experimental structure and its match within each CSP set, and the relative energy of the match to the experimental structure.

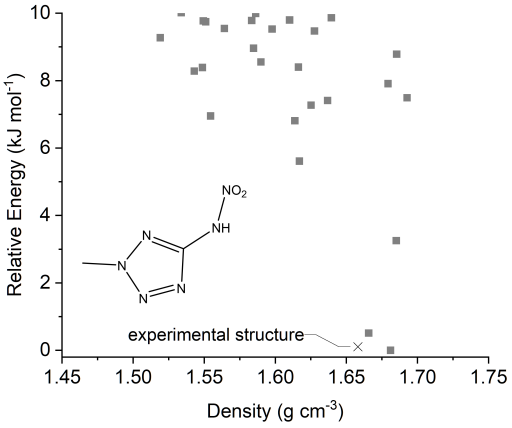

(a)

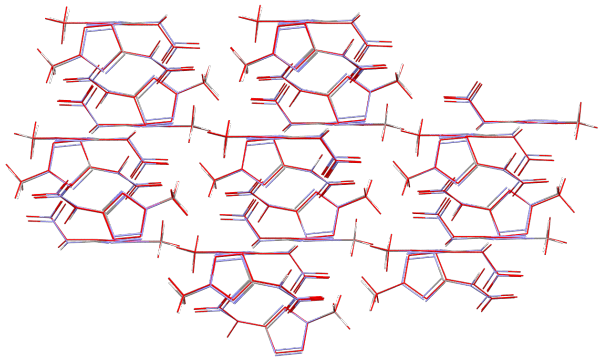

(b)

Figure 3: An example CSP result for MNT generated using the FIT force field and the PBE0/aug-cc-pVTZ electrostatic model. (a) The CSP landscape for MNT, where each data point represents a predicted crystal structure. The predicted structure that matches the experimentally observed structure is labeled and indicated by a black cross. Relative energy represents the energy gap between each data point and the global energy minimum. (b) An overlay of the experimental structure (shown with element colors) and the closest predicted match to the experimental structure (red). The $RMSD_{30}$ for this overlay is 0.190 Å.

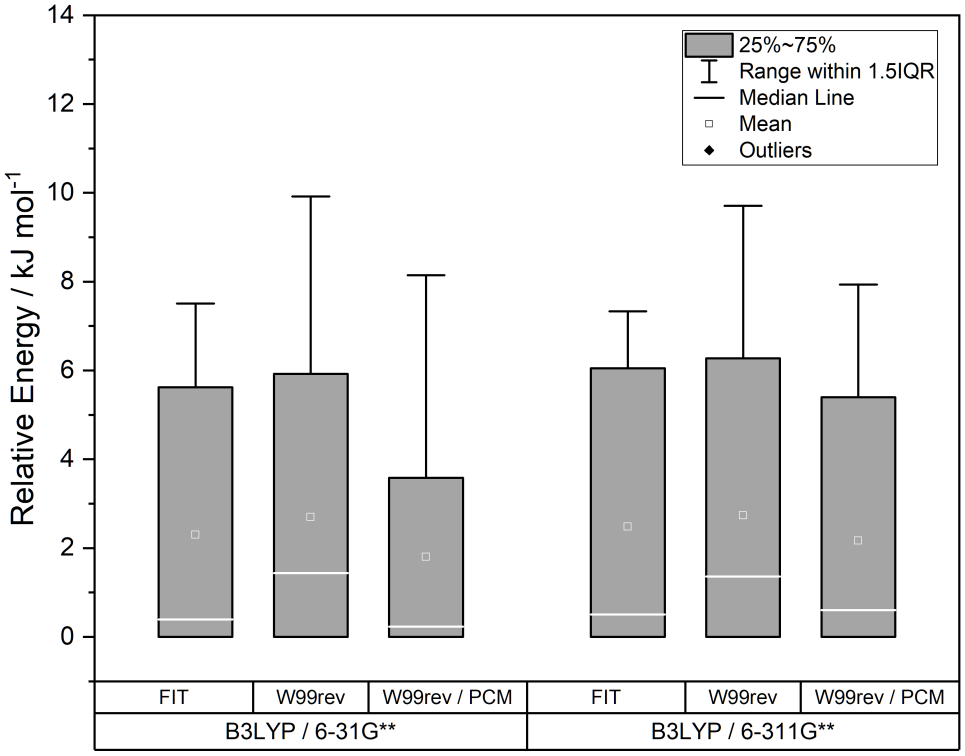
25%~75%
Range within 1.5IQR
Median Line
Mean
Outliers
Relative Energy / kJ mol-1
0
2
4
6
8
10
12
14
FIT
W99rev
W99rev / PCM
FIT
W99rev
W99rev / PCM
B3LYP / 6-31G**
B3LYP / 6-311G**

(a)

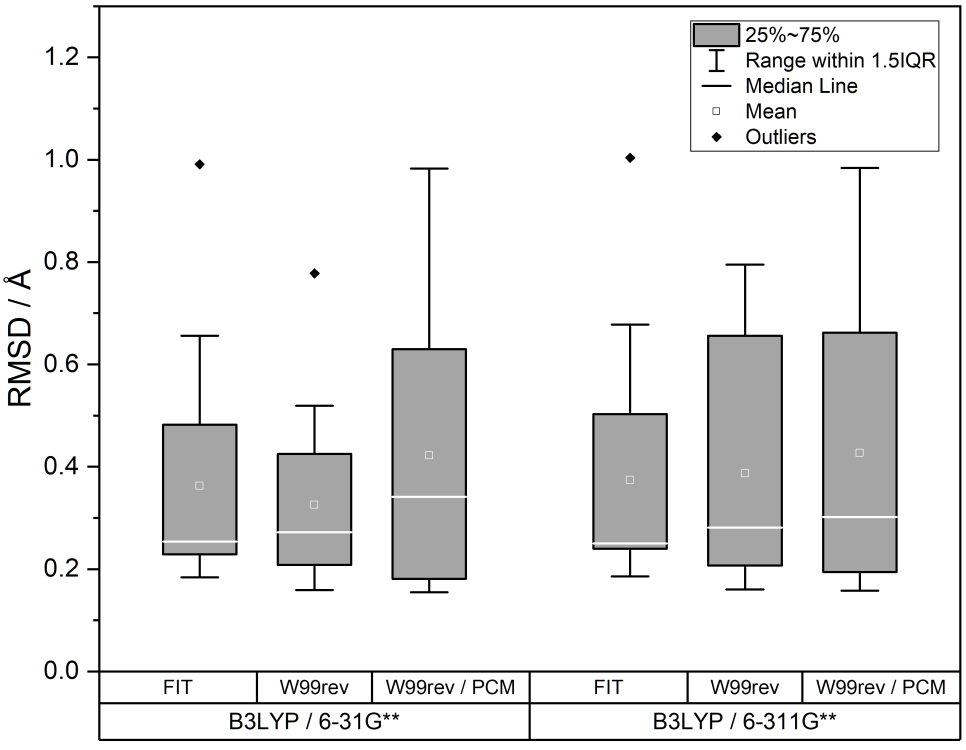
25%~75%
Range within 1.5IQR
Median Line
Mean
Outliers
RMSD / Å
0.0
0.2
0.4
0.6
0.8
1.0
1.2
FIT
W99rev
W99rev / PCM
FIT
W99rev
W99rev / PCM
B3LYP / 6-31G**
B3LYP / 6-311G**

(b)

Figure 4: Box plots showing the results of 60 total CSPs: six combinations of force field and electrostatic model for the 10 EMs shown in Figure 1. B3LYP/6-31G** and B3LYP/6-311G** were used to model the atomic multipoles in order to stay consistent with the electrostatic model used to parameterize W99rev. For each force field / electrostatic model combination, 11 total comparisons were performed between predicted crystal structures and experimentally known polymorphs. ATZ and α-FOX-7 are not included in these results due to the flexible NH_2 groups not being well modelled by the rigid-molecule calculations (as detailed in the SI). β-FOX-7 was included as the NH_2 conformation within the experimental structure matched the conformation within the DFT optimized geometry used in CSP. HMX has two conformers of the 8-membered ring (referred to as chair and chair-chair), which were treated as separate CSPs in these summary results due to the large conformational energy difference. (a) shows the distribution of relative energies (the energy difference between the predicted match to the experimental crystal structure and the global energy minimum) for all predicted matches to their respective experimentally known polymorph. (b) shows the distribution of $RMSD_{30}$ between for all predicted matches to their respective experimentally known polymorph.

The best performing force field and electrostatic model combination is that which minimizes the $RMSD_{30}$, which measures structural deviations between predicted and experimental crystal structures, and ranks the matches to the observed crystal structures well (low energies relative to the global energy minimum). No choice of force field emerges from this study as performing better than the others by both measures. The best force field at ranking energies of the observed crystal structures (W99rev + B3LYP/6-31G**(PCM)) produces the largest geometric deviations, whereas that producing the smallest range of $RMSD_{30}$ (W99rev + B3LYP/6-31G**) gives the worst overall performance on energy ranking. Without a clear optimum from these results, we proceed with the FIT force field, which produces a small range in $RMSD_{30}$ and low median relative energies in these tests, and performs best in previous benchmarks against measured sublimation enthalpies for a variety of small organic crystal systems.[13]

Choice of Electrostatic Model

We also examined the sensitivity of CSP results to the charge density used to derive the electrostatic model by comparing the CSP results obtained from atomic multipoles generated

by HF, MP2 and the DFT functionals PBE, PBE0 and B3LYP with the Dunning basis sets: aug-cc-pVDZ and aug-cc-pVTZ. 6-31G** and 6-311G** basis sets are present with B3LYP since they were used in the initial force field evaluation presented in the previous section.

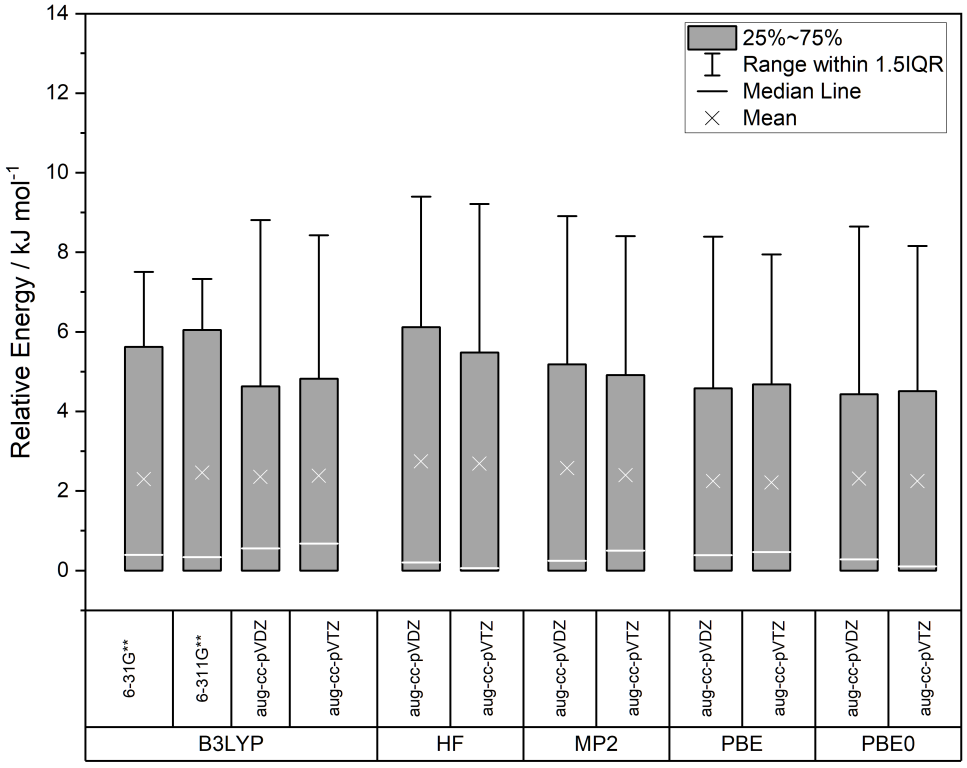
25%~75%
Range within 1.5IQR
Median Line
Mean
Relative Energy / kJ mol-1
0
2
4
6
8
10
12
14
6-31G**
6-311G**
aug-cc-pVDZ
aug-cc-pVTZ
B3LYP
HF
MP2
PBE
PBE0

(a)

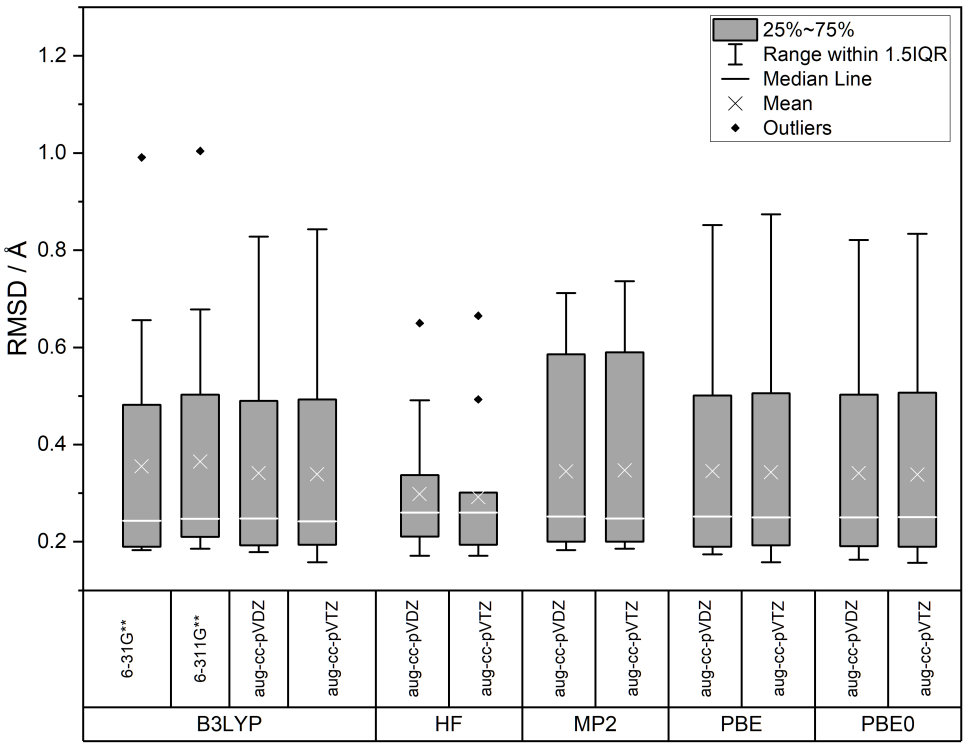
25%~75%
Range within 1.5IQR
Median Line
Mean
Outliers
RMSD / Å
0.2
0.4
0.6
0.8
1.0
1.2
6-31G**
6-311G**
aug-cc-pVDZ
aug-cc-pVTZ
B3LYP
HF
MP2
PBE
PBE0

(b)

Figure 5: Box Plots showing the results of 120 total CSPs, 12 combinations of DFT functional and basis set for the 10 EMs shown in Figure 1. For each electrostatic model, 11 total comparisons were performed between predicted crystal structures and experimentally known polymorphs. ATZ and α-FOX-7 are not included in these results due to the flexible NH_2 groups not being well modelled by the rigid-molecule calculations (as detailed in the SI). β-FOX-7 was included as the NH_2 conformation within the experimental structure matched the conformation within the DFT optimized geometry used in CSP. HMX has two conformers (referred to as chair and chair-chair), which were treated as separate CSPs in these summary results due to the large conformational energy difference. (a) the distribution of relative energies (the energy difference between the predicted match and the global energy minimum) for all 13 predicted matches to their respective experimentally known polymorph. (b) the distribution of $RMSD_{30}$ between for all 13 predicted matches to their respective experimentally known polymorph.

The electrostatic models were evaluated analogously to the force fields, by comparing $RMSD_{30}$ and relative energies for predicted crystal structures that match the experimental structures across the molecules in the test set. HF performs surprisingly well on geometries, which might be due to cancellation of errors (HF exaggeration of charge separation could make up for the lack of explicit polarization in the force field method), but gives among the largest ranges for relative energies. The higher cost of MP2 calculations does not lead to better results than DFT-based electrostatic models. The results are similar among the DFT methods tested, showing that the average performance of CSP is not particularly sensitive to the functional and basis set from which the electrostatic model is derived.

We chose PBE0/aug-cc-pVTZ to generate our electrostatic model in our final force field-based CSP results. We chose this electrostatic model as it represents a balance between high accuracy and for close consistency of DFT functional with the PBE functional in our subsequent periodic DFT calculations. We chose aug-cc-pVTZ as our basis set as in combination with PBE0, it is computationally affordable for all our molecules. If CSP was being performed on larger molecules, this basis set could be reduced without affecting the quality of the CSP, as shown with these results.

Detailed CSP Results

Table 1 details our CSP results for both the force field landscapes and periodic DFT optimized landscapes; it provides the numerical ranking, relative energy and $RMSD_{30}$ for each of the CSP matches to the experimental structures for all of the Z' = 1 polymorphs of the ten EMs (Figure 1).

For comparison with the force field-based results, we also summarize the results of periodic DFT re-optimizations of the low energy crystal structures. To generate the DFT-based CSP results, all force field predicted structures within 10 kJ mol^{-1} of the global energy minimum for each of the ten EMs were re-optimized. For ATZ the energy window was increased to 12 kJ mol^{-1} as the experimental match was found at 11.46 kJ mol^{-1}; ATZ is an outlier in our overall results, which we discuss further below. For HMX, due to the large molecular energy difference between chair and chair-chair conformers, we performed peroidic DFT on the lowest 10 kJ mol^{-1} for each conformer. FOX-7, HMX and NTO all possess an experimental polymorph with Z' > 1. Thus, to examine where these would occur in energy if CSP had been performed with higher Z', the experimental structures were independently optimized using the force field (FIT with PBE0/aug-cc-pVTZ multipoles) and periodic DFT and their numerical ranking and relative energies, after each stage of optimization, are shown in Table 1. Note that for these polymorphs, the numerical ranking and relative energies are lower bounds on what they would be if CSP searches had included high Z'.

Table 1: CSP results for the landscapes of the 10 EMs shown in Figure 1 produced using the FIT force field and PBE0/aug-cc-pVTZ atomic multipoles. The numerical ranking is the energy-ranked position of the match to the experimental structure within the list of CSP structures. Relative energy is the energy gap between each EM's predicted global energy minimum and the CSP match to the experimental structure. $RMSD_{30}$ represents the quality of our predicted matched structure when compared to the experimental structure: a low value corresponds to a higher quality match. $RMSD_{30}$ values were obtained via a COMPACK comparison using 30% distance tolerances and 30° angle tolerances. For HMX, the two conformers possess a large intramolecular energy difference of 12.84 kJ mol^{-1} and thus for α-HMX and δ-HMX we report the numerical ranking and relative energy within the CSP of the individual conformer as a number in parentheses for the force field columns (DFT accounts for this intramolecular energy difference and thus the issue does not apply here). γ-FOX-7, ϵ-HMX and α-NTO possess a Z' > 1 and are thus shaded grey in the table.

Energetic Material	CSD Refcode	Force Field			Solid State DFT		
		Rank	E_{rel} / kJ mol^{-1}	$RMSD_{30}$ / Å	Rank	E_{rel} / kJ mol^{-1}	$RMSD_{30}$ / Å
ABT	EWEYEL	1	0	0.166	1	0	0.097
ATZ	EJIQEU	221	11.46	0.612	113	9.06	0.492
DNIT	VIWRAV	15	4.51	0.507	1	0	0.316
α-FOX-7	SEDTUQ11	186	9.66	0.299	2	0.50	0.177
β-FOX-7	SEDTUQ06	16	3.49	0.254	3	0.67	0.174
γ-FOX-7	SEDTUQ25	51	5.64	-[1]	32	3.22	0.033[2]
HBT	TIPZAU	1	0	0.655	1	0	0.389
α-HMX	OCHTET	86 (1)	19.83 (0.0)	0.255	1	0	0.048
β-HMX	OCHTET13	2	1.44	0.231	2	3.00	0.085
δ-HMX	OCHTET03	335 (39)	27.86 (8.04)	0.224	9	5.65	0.116
ϵ-HMX	OCHTET22	1	0	0.211[2]	3	3.29	0.044[2]
HNB	HNOBEN	1	0	0.251	2	0.78	0.157
MNT	VITBAC	2	0.10	0.190	1	0	0.110
α-NTO	QOYJOD06	7	4.83	0.195[2]	3	3.99	0.024[2]
β-NTO	QOYJOD09	18	8.16	0.834	2	1.50	0.739
TATB	TATNBZ03	3	0.92	0.157	2	0.12	0.124

[1] γ-FOX-7 has two distinct conformations in its asymmetric unit and thus our gas phase minimum geometry does not match one of the two conformations. This has altered the quality of our RMSD but this would be resolved if a CSP was carried out for an asymmetric unit of two FOX-7 molecules with multiple conformations.

[2] γ-FOX-7, ϵ-HMX and α-NTO are highlighted in grey as they have more then one molecule in the asymmetric unit cell and so they were not found in our CSP (which was restricted to one molecule in the asymmetric unit cell). Thus the experimental structures were optimized through the force field and solid state DFT individually; in order to identify where they lie on their respective landscapes.

Force field CSP results

The rigid-molecule force field-based CSP performs well at reproducing many of the known crystal structures with low RMSD and good energetic ranking, although the results are more variable than when similar methods are applied for non-EM molecular crystals.[72] This demonstrates the power of a force field based model as a simple and fast method which can produce accurate predictions for crystal structures. Geometrically, the known crystal structures are reproduced well, with small RMSD in atomic positions. Only ATZ, DNIT, HBT and β-NTO have $RMSD_{30}$ values above 0.5 Å.

Energetically, the rigid-molecule force field CSP results are mixed. A main assumption of CSP is that observed crystal structures will correspond to low energy structures; a perfect prediction corresponds to the known structures matching the global minimum (rank = 1) structure, or the lowest set of structures for polymorphic molecules. We observe excellent rankings for several of the EMs (ABT, HBT, HNB, MNT, TATB and the β and ϵ polymorphs of HMX, which adopt the lower energy chair conformer). However, several of the matches to known crystal structures are energetically ranked poorly at the force field level, which we attribute to the rigid-molecule approximation more than the quality of the intermolecular force field itself.

The relatively poor energetic rankings for ATZ and FOX-7 are likely related to the flexibility of the NH_2 groups causing mismatches between our gas-phase optimized geometry and the molecular geometry within the experimental crystal structures. For HMX, the α and δ polymorphs are ranked poorly. Both of these polymorphs contain the chair-chair HMX conformer and although α-HMX corresponds to the lowest energy predicted structure from the chair-chair conformation, it is far above the global minimum in total energy. The HMX results show that the mixed force field intermolecular energy + DFT conformational energy model (Equation 1) does not work well in this case.

The poor results for NTO are not fully understood. Although the choice of force field and electrostatic model was not found to influence the average CSP performance across all

EMs, we observed that the results for individual molecules could be sensitive to the choice of force field. For example, CSP using the W99rev force field with B3LYP/6-311G** provided a match to the experimental β-NTO crystal structure with an $RMSD_{30}$ of 0.281 Å (see SI for more detail) and a relative energy of 1.98 kJ mol^{-1}.

DFT re-ranked CSP results

The results are systematically improved by DFT (PBE-GD3BJ) reoptimization, after which five (ABT, DNIT, HBT, α-HMX, MNT) of the known crystal structures are predicted as the global energy minimum on their respective CSP landscape, and a further eight as the second or third lowest energy structures (Table 1).

Of the EMs that performed poorly in the rigid-molecule force field CSP, results for NTO are improved significantly, ranking the α and β polymorphs as 3rd and 2nd lowest energy structures, ranking of the FOX-7 polymorphs is improved such that the known polymorphs are 2nd, 3rd and 32nd lowest energy structures, and HMX predictions now place the four known polymorphs as 1st, 2nd, 3rd and 9th ranked in energy. The HMX results demonstrate that the high molecular energy of the chair-chair conformation can be compensated by improved interactions in the solid state. The energy range of all of the polymorphic EMs falls well within the range normally seen for organic molecular polymorphs.[73]

Only three out of the 16 experimentally observed crystal structures being ranked outside the three lowest energy predictions with γ-FOX-7 and ATZ being worst ranked, as 32nd and 113th ranked structures by energy after DFT re-optimization.

The only EMs with $RMSD_{30}$ values above 0.4 Å after DFT re-optimization are ATZ and β-NTO. These matches could be cross-checked with other similarity measures,[74] but we check them here by visual inspection. The higher $RMSD_{30}$ matches are still plausibly close, as displayed in Figure 6b and Figure 6c respectively. For comparison, the quantitatively much closer agreement for ABT is also depicted in Figure 6a.

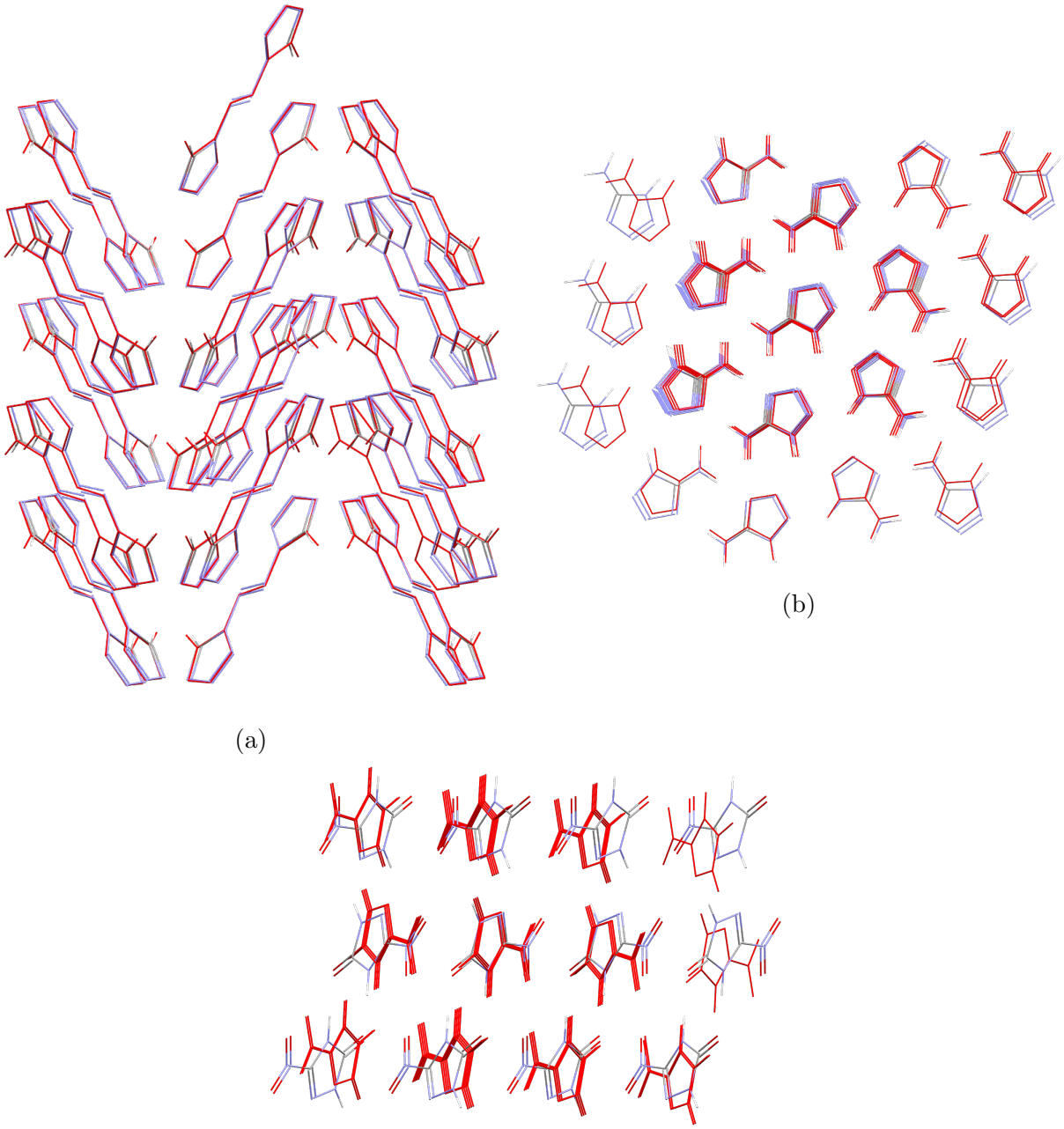

Figure 6: Visualization of the $COMPACK_{30}$ comparison between the experimental structures of (a) ABT ($RMSD_{30} = 0.097$ Å), (b) ATZ ($RMSD_{30} = 0.492$ Å) and (c) β-NTO ($RMSD_{30} = 0.739$ Å) and the respective predicted matches to the experimental structures found by CSP after DFT re-optimization. The experimental structure is shown with colouring by element and the predicted match is shown in full red colouring.

Further explorations of ATZ

The clearest outlier among the DFT results is ATZ, whose crystal structure is poorly ranked by energy (9 kJ mol^{-1} above the global energy minimum from CSP) and with one of the worst geometric matches to the experimentally determined structure ($RMSD_{30}$ = 0.492 Å). A series of additional calculations were performed to better understand this apparent failure of force field and DFT-based CSP to identify the observed crystal structure as a low-energy structure for this molecule.

The reported crystal structure of ATZ has a planar NH_2 group, whereas the NH_2 is pyramidalized in the DFT optimized molecular geometry used in CSP (see Figure S24, ESI). Although solid state DFT re-optimization should allow the hydrogens to find their energetically most favourable orientations within each crystal structure, we repeated CSP starting with a molecular geometry constrained to be planar. These constraints made minimal difference to the final CSP predictions (see SI Table S15 for more details); the known structure remained high in energy on the resulting CSP landscape.

To test whether the CSP structure generation had failed to locate the local energy minimum nearest to the observed crystal structure, we performed lattice energy minimization (using FIT multipoles) on the experimentally determined crystal structure after replacing the molecular geometry by the DFT gas phase optimized molecule. The obtained structure was virtually identical to the predicted structures obtained from CSP. This result confirmed that the structure found during CSP is the nearest local energy minimum to the observed crystal structure. The same test was performed with β-NTO, with the same result. For both molecules, further sampling during CSP structure generation would not find a better match to the observed crystal structure.

The structure report for ATZ[23] had some uncertainty in the hydrogen position defining the tautomer, as the structure was determined from powder diffraction data. Our initial CSP assumed the 1H-tautomer, as shown in Figure 1. We ran CSP with the 2H-tautomer of ATZ (see SI for further details) to determine if the alternative tautomer would lead to a

lower energy or closer geometric match to the experimental solution; the known structure forms hydrogen bonds between the N1 and N2 positions in the ring, so the 2H-tautomer could plausibly form the same crystal packing with the H atom shifted across the hydrogen bond. CSP with the 2H-tautomer does produce matches to the packing of the known crystal structure. However, after DFT re-optimization (PBE-GD3BJ), the energies of these structures were found to be more than 11.5 kJ mol^{-1} above the matches found with the 1H-tautomer (see Figure S29). Thus, including the alternative tautomer of ATZ does not improve the CSP results for this molecule.

As a final test, we tested whether the poor energy ranking of the ATZ crystal structure is a limitation of the GGA functional used in DFT re-optimization of structures. 11 CSP structures, including the global energy minimum, of ATZ were selected from the DFT re-optimized set, evenly sampling the low energy range. Single-point PBE0 calculations were performed with the GD3BJ dispersion correction to assess the extent of re-ranking by changing to a hybrid DFT functional. The reranking was found to be up to a few kJ mol^{-1} (see Figure S29), which lowered the relative energy of the match to the experimental structure to 5.65 kJ mol^{-1} (among this subset of structures). PBE0 energy calculations did not significantly affect the relative energies of structures with the 2H-tautomer compared to the 1H tautomer. These results hint that the outlier results for ATZ could be due to limitations of GGA functionals, which are known to suffer from self-interaction error.[75] However, it is plausible that the reported experimental crystal structure of ATZ is in fact a meta-stable polymorph and the true thermodynamically stable polymorph is present within our predicted landscape; there is a growing number of examples where CSP has suggested polymorphs that have subsequently been realized experimentally.[17,18,20,76]

Conclusion

We have evaluated crystal structure prediction by global exploration of the lattice energy surface on a set of ten highly energetic organic molecules. The computational methodology applied a rigid-molecule approach using an empirical force field with atomic multipole electrostatics, followed by re-optimization of the lowest energy predicted structures using dispersion-corrected solid state DFT. The results demonstrate that this is a reliable approach for structure prediction of this class of energetic materials.

The rigid-molecule, force field-based CSP approach provides useful results. Matches within the CSP results are found for all of the known Z'=1 crystal structures and, for four of the ten molecules, the predicted global energy minimum corresponds to the known crystal structure, or one of the known polymorphs. Many of the other experimentally observed crystal structures correspond to predicted structures with low numerical ranks in the energy-ordered sets of predictions. Therefore, this approach can act as a first stage in CSP, which provides a small set of structures for re-optimization at a higher level of theory.

Solid state DFT re-optimization of CSP structures produces excellent CSP results; of the 13 target experimentally-determined Z'=1 crystal structures of the ten molecules, 10 are reproduced with excellent quality, within the 3 lowest energy predicted structures, and with $RMSD_{30}$ to the experimental structure below 0.4 Å. Two of the other structures showed either slightly higher energy (δ-HMX) or worse geometric agreement with the experimentally-determined structure (β-NTO), and the known crystal structure of ATZ remained poorly predicted after DFT. We believe that the result for ATZ is due, at least in part, to limitations of the GGA DFT functional.

Thus, we demonstrate CSP as a reliable tool for the development and screening of EMs. We envision that CSP could be carried out in future to guide screening efforts for polymorphs of energetic molecules. The reliability of structure prediction methods also provides a route to the anticipation of materials properties in advance of molecular synthesis, which could be achieved by combining CSP with methods for evaluating, for example, impact sensitivities.[10]

Acknowledgement

J.E.A. and G.M.D. thank the Air Force Office of Scientific Research for funding under award no. FA8655-20-1-7000. We acknowledge the use of the IRIDIS High Performance Computing Facility, and associated support services at the University of Southampton, in the completion of this work. We are grateful to the UK Materials and Molecular Modelling Hub for computational resources on the national HPC Young, which is partially funded by EPSRC (EP/P020194/1 and EP/T022213/1).

J.E.A. gratefully acknowledges Dr Christopher R Taylor for his assistance throughout this work and Myles T. Blurton for his assistance with creating many of the figures we have presented.

Supporting Information Available

CIF files with all re-optimised structures for each EM are available at https://doi.org/10.5258/SOTON/D26
Supporting information also includes: tables with relative energies and $RMSD_{30}$ values from choice of force field and electrostatic model sections; CSP landscapes for each EM and visualizations of each predicted match to the experimental structures; further details on our investigations into the results from ATZ, α-FOX-7 and β-NTO.

References

(1) Zlotin, S. G.; Churakov, A. M.; Egorov, M. P.; Fershtat, L. L.; Klenov, M. S.; Kuchurov, I. V.; Makhova, N. N.; Smirnov, G. A.; Tomilov, Y. V.; Tartakovsky, V. A. Advanced energetic materials: novel strategies and versatile applications. *Mendeleev Communications* **2021**, *31*, 731–749.

(2) Zhao, G.; Yin, P.; Staples, R.; Shreeve, J. M. One-step synthesis to an insensitive ex-

plosive: N,N-bis((1H-tetrazol-5-yl)methyl)nitramide (BTMNA). *Chemical Engineering Journal* **2021**, *412*, 128697.

(3) Zhang, J.; Mitchell, L. A.; Parrish, D. A.; Shreeve, J. M. Enforced Layer-by-Layer Stacking of Energetic Salts towards High-Performance Insensitive Energetic Materials. *Journal of the American Chemical Society* **2015**, *137*, 10532–10535.

(4) Wang, X.; Xu, K.; Sun, Q.; Wang, B.; Zhou, C.; Zhao, F. The Insensitive Energetic Material Trifurazano-oxacycloheptatriene (TFO): Synthesis and Detonation Properties. *Propellants, Explosives, Pyrotechnics* **2015**, *40*, 9–12.

(5) Xu, J.-G.; Li, X.-Z.; Wu, H.-F.; Zheng, F.-K.; Chen, J.; Guo, G.-C. Substitution of Nitrogen-Rich Linkers with Insensitive Linkers in Azide-Based Energetic Coordination Polymers toward Safe Energetic Materials. *Crystal Growth & Design* **2019**, *19*, 3934–3944.

(6) Fischer, N.; Klapötke, T. M.; Scheutzow, S.; Stierstorfer, J. Hydrazinium 5-Aminotetrazolate: an Insensitive Energetic Material Containing 83.72% Nitrogen. *Central European Journal of Energetic Materials* **2008**, *5*, 3–18.

(7) Xue, Q.; Bi, F.-q.; Zhang, J.-l.; Wang, Z.-j.; Zhai, L.-j.; Huo, H.; Wang, B.-z.; Zhang, S.-y. A Family of Energetic Materials Based on 1,2,4-Oxadiazole and 1,2,5-Oxadiazole Backbones With Low Insensitivity and Good Detonation Performance. *Frontiers in Chemistry* **2020**, *7*.

(8) Tang, Y.; He, C.; Imler, G. H.; Parrish, D. A.; Shreeve, J. M. Aminonitro Groups Surrounding a Fused Pyrazolotriazine Ring: A Superior Thermally Stable and Insensitive Energetic Material. *Applied Energy Materials* **2019**, *2*, 2263–2267.

(9) Sun, Q.; Li, X.; Lin, Q.; Lu, M. Tetracyclic pyrazine-fused furazans as insensitive energetic materials: syntheses, structures, and properties. *Org. Biomol. Chem.* **2018**, *16*, 8034–8037.

(10) Michalchuk, A. A.; Trestman, M.; Rudić, S.; Portius, P.; Fincham, P. T.; Pulham, C. R.; Morrison, C. A. Predicting the reactivity of energetic materials: An: ab initio multiphonon approach. *Journal of Materials Chemistry A* **2019**, *7*, 19539–19553.

(11) Price, S. L. Is zeroth order crystal structure prediction (CSP0) coming to maturity? What should we aim for in an ideal crystal structure prediction code? *Faraday Discuss.* **2018**, *211*, 9–30.

(12) Woodley, S. M.; Day, G. M.; Catlow, R. Structure prediction of crystals, surfaces and nanoparticles. *Philosophical Transactions of the Royal Society A: Mathematical, Physical and Engineering Sciences* **2020**, *378*, 20190600.

(13) Nyman, J.; Pundyke, O. S.; Day, G. M. Accurate force fields and methods for modelling organic molecular crystals at finite temperatures. *Phys. Chem. Chem. Phys.* **2016**, *18*, 15828–15837.

(14) Otero-de-la Roza, A.; Johnson, E. R. A benchmark for non-covalent interactions in solids. *The Journal of Chemical Physics* **2012**, *137*, 054103.

(15) Reilly, A. M.; Tkatchenko, A. Understanding the role of vibrations, exact exchange, and many-body van der Waals interactions in the cohesive properties of molecular crystals. *The Journal of Chemical Physics* **2013**, *139*, 024705.

(16) Maurer, R. J.; Freysoldt, C.; Reilly, A. M.; Brandenburg, J. G.; Hofmann, O. T.; Björkman, T.; Lebègue, S.; Tkatchenko, A. Advances in Density-Functional Calculations for Materials Modeling. *Annual Review of Materials Research* **2019**, *49*, 1–30.

(17) Neumann, M. A.; van de Streek, J.; Fabbiani, F. P. A.; Hidber, P.; Grassmann, O. Combined crystal structure prediction and high-pressure crystallization in rational pharmaceutical polymorph screening. *Nature Communications* **2015**, *6*, 7793.

(18) Taylor, C. R.; Mulvee, M. T.; Perenyi, D. S.; Probert, M. R.; Day, G. M.; Steed, J. W. Minimizing Polymorphic Risk through Cooperative Computational and Experimental Exploration. *Journal of the American Chemical Society* **2020**, *142*, 16668–16680.

(19) Aitchison, C. M.; Kane, C. M.; McMahon, D. P.; Spackman, P. R.; Pulido, A.; Wang, X.; Wilbraham, L.; Chen, L.; Clowes, R.; Zwijnenburg, M. A.; Sprick, R. S.; Little, M. A.; Day, G. M.; Cooper, A. I. Photocatalytic proton reduction by a computationally identified, molecular hydrogen-bonded framework. *J. Mater. Chem. A* **2020**, *8*, 7158–7170.

(20) Pulido, A. et al. Functional materials discovery using energy–structure–function maps. *Nature* **2017**, *543*, 657–664.

(21) Bier, I.; O'Connor, D.; Hsieh, Y.-T.; Wen, W.; Hiszpanski, A. M.; Han, T. Y.-J.; Marom, N. Crystal structure prediction of energetic materials and a twisted arene with Genarris and GAtor. *CrystEngComm* **2021**, *23*, 6023–6038.

(22) Klapötke, T. M.; Piercey, D. G. 1,1-Azobis(tetrazole): A Highly Energetic Nitrogen-Rich Compound with a N10 Chain. *Inorganic Chemistry* **2011**, *50*, 2732–2734.

(23) Fujihisa, H.; Honda, K.; Obata, S.; Yamawaki, H.; Takeya, S.; Gotoh, Y.; Matsunaga, T. Crystal structure of anhydrous 5-aminotetrazole and its high-pressure behavior. *CrystEngComm* **2011**, *13*, 99–102.

(24) Klapötke, T.; Stierstorfer, J. Nitration Products of 5-Amino-1H-tetrazole and Methyl-5-amino-1H-tetrazoles – Structures and Properties of Promising Energetic Materials. *Helvetica Chimica Acta* **2007**, *90*, 2132–2150.

(25) Evers, J.; Klapötke, T. M.; Mayer, P.; Oehlinger, G.; Welch, J. α- and β-FOX-7, Polymorphs of a High Energy Density Material, Studied by X-ray Single Crystal and Powder Investigations in the Temperature Range from 200 to 423 K. *Inorganic Chemistry* **2006**, *45*, 4996–5007.

(26) Meents, A.; Dittrich, B.; Johnas, S. K. J.; Thome, V.; Weckert, E. F. Charge-density studies of energetic materials: CL-20 and FOX-7. *Acta Crystallographica Section B* **2008**, *64*, 42–49.

(27) Woińska, M.; Grabowsky, S.; Dominiak, P. M.; Woźniak, K.; Jayatilaka, D. Hydrogen atoms can be located accurately and precisely by x-ray crystallography. *Science Advances* **2016**, *2*, e1600192.

(28) Crawford, M.-J.; Evers, J.; Göbel, M.; Klapötke, T. M.; Mayer, P.; Oehlinger, G.; Welch, J. M. γ-FOX-7: Structure of a High Energy Density Material Immediately Prior to Decomposition. *Propellants, Explosives, Pyrotechnics* **2007**, *32*, 478–495.

(29) Klapötke, T. M.; Sabaté, C. M. 5,5-Hydrazinebistetrazole: An Oxidation-stable Nitrogen-rich Compound and Starting Material for the Synthesis of 5,5-Azobistetrazolates. *Zeitschrift für anorganische und allgemeine Chemie* **2007**, *633*, 2671–2677.

(30) Cady, H. H.; Larson, A. C.; Cromer, D. T. The crystal structure of α-HMX and a refinement of the structure of β-HMX. *Acta Crystallographica* **1963**, *16*, 617–623.

(31) Zhurova, E. A.; Zhurov, V. V.; Pinkerton, A. A. Structure and Bonding in -HMX-Characterization of a Trans-Annular N···N Interaction. *Journal of the American Chemical Society* **2007**, *129*, 13887–13893.

(32) Cobbledick, R. E.; Small, R. W. H. The crystal structure of the δ-form of 1,3,5,7-tetranitro-1,3,5,7-tetraazacyclooctane (δ-HMX). *Acta Crystallographica Section B* **1974**, *30*, 1918–1922.

(33) Korsunskii, B. L.; Aldoshin, S. M.; Vozchikova, S. A.; Golovina, N. I.; Chukanov, N. V.; Shilov, G. V. A new crystalline HMX Polymorph: -HMX. *Russian Journal of Physical Chemistry B* **2010**, *4*, 934–941.

(34) Klapötke, T.; Stierstorfer, J. Nitration Products of 5-Amino-1H-tetrazole and Methyl-5-amino-1H-tetrazoles – Structures and Properties of Promising Energetic Materials. *Helvetica Chimica Acta* **2007**, *90*, 2132–2150.

(35) Zhurova, E. A.; Pinkerton, A. A. Chemical bonding in energetic materials: β-NTO. *Acta Crystallographica Section B* **2001**, *57*, 359–365.

(36) Bolotina, N.; Kirschbaum, K.; Pinkerton, A. A. Energetic materials: α-NTO crystallizes as a four-component triclinic twin. *Acta Crystallographica Section B* **2005**, *61*, 577–584.

(37) Cady, H. H.; Larson, A. C. The crystal structure of 1,3,5-triamino-2,4,6-trinitrobenzene. *Acta Crystallographica* **1965**, *18*, 485–496.

(38) Chua, Z.; Gianopoulos, C. G.; Zarychta, B.; Zhurova, E. A.; Zhurov, V. V.; Pinkerton, A. A. Inter- and Intramolecular Bonding in 1,3,5-Triamino-2,4,6-trinitrobenzene: An Experimental and Theoretical Quantum Theory of Atoms in Molecules (QTAIM) Analysis. *Crystal Growth & Design* **2017**, *17*, 5200–5207.

(39) Case, D. H.; Campbell, J. E.; Bygrave, P. J.; Day, G. M. Convergence Properties of Crystal Structure Prediction by Quasi-Random Sampling. *Journal of Chemical Theory and Computation* **2016**, *12*, 910–924.

(40) Frisch, M. J. et al. Gaussian˜16 Revision C.01. 2016; Gaussian Inc. Wallingford CT.

(41) Brill, T. B.; Reese, C. O. Analysis of intra- and intermolecular interactions relating to the thermophysical behavior of .alpha.-, .beta.-, and .delta.-octahydro-1,3,5,7-tetranitro-1,3,5,7-tetraazocine. *The Journal of Physical Chemistry* **1980**, *84*, 1376–1380.

(42) Price, S. L.; Leslie, M.; Welch, G. W. A.; Habgood, M.; Price, L. S.; Karamertzanis, P. G.; Day, G. M. Modelling organic crystal structures using distributed multipole

and polarizability-based model intermolecular potentials. *Phys. Chem. Chem. Phys.* **2010**, *12*, 8478–8490.

(43) Coombes, D. S.; Price, S. L.; Willock, D. J.; Leslie, M. Role of Electrostatic Interactions in Determining the Crystal Structures of Polar Organic Molecules. A Distributed Multipole Study. *The Journal of Physical Chemistry* **1996**, *100*, 7352–7360.

(44) Pyzer-Knapp, E. O.; Thompson, H. P. G.; Day, G. M. An optimized intermolecular force field for hydrogen-bonded organic molecular crystals using atomic multipole electrostatics. *Acta Crystallographica Section B* **2016**, *72*, 477–487.

(45) Becke, A. D. Density-functional thermochemistry. III. The role of exact exchange. **1993**, *98*, 5648–5652.

(46) Stephens, P. J.; Devlin, F. J.; Chabalowski, C. F.; Frisch, M. J. Ab Initio Calculation of Vibrational Absorption and Circular Dichroism Spectra Using Density Functional Force Fields. *The Journal of Physical Chemistry* **1994**, *98*, 11623–11627.

(47) Francl, M. M.; Pietro, W. J.; Hehre, W. J.; Binkley, J. S.; Gordon, M. S.; DeFrees, D. J.; Pople, J. A. Selfâ€consistent molecular orbital methods. XXIII. A polarizationâ€type basis set for secondâ€row elements. *The Journal of Chemical Physics* **1982**, *77*, 3654–3665.

(48) McLean, A. D.; Chandler, G. S. Contracted Gaussian basis sets for molecular calculations. I. Second row atoms, Z=11â€“18. *The Journal of Chemical Physics* **2008**, *72*, 5639–5648.

(49) Mennucci, B.; Tomasi, J. Continuum solvation models: A new approach to the problem of soluteâ€™s charge distribution and cavity boundaries. *The Journal of Chemical Physics* **1997**, *106*, 5151–5158.

(50) Cooper, T. G.; Hejczyk, K. E.; Jones, W.; Day, G. M. Molecular Polarization Effects on the Relative Energies of the Real and Putative Crystal Structures of Valine. *Journal of Chemical Theory and Computation* **2008**, *4*, 1795–1805, PMID: 26620182.

(51) Stone, A.; Alderton, M. Distributed multipole analysis. *Molecular Physics* **1985**, *56*, 1047–1064.

(52) Stone, A. J. Distributed Multipole Analysis: Stability for Large Basis Sets. *Journal of Chemical Theory and Computation* **2005**, *1*, 1128–1132.

(53) Roothaan, C. C. J. New Developments in Molecular Orbital Theory. *Rev. Mod. Phys.* **1951**, *23*, 69–89.

(54) Møller, C.; Plesset, M. S. Note on an Approximation Treatment for Many-Electron Systems. *Phys. Rev.* **1934**, *46*, 618–622.

(55) Perdew, J. P.; Burke, K.; Ernzerhof, M. Generalized Gradient Approximation Made Simple. *Phys. Rev. Lett.* **1996**, *77*, 3865–3868.

(56) Perdew, J. P.; Burke, K.; Ernzerhof, M. Generalized Gradient Approximation Made Simple [Phys. Rev. Lett. 77, 3865 (1996)]. *Phys. Rev. Lett.* **1997**, *78*, 1396–1396.

(57) Adamo, C.; Barone, V. Toward reliable density functional methods without adjustable parameters: The PBE0 model. **1999**, *110*, 6158–6170.

(58) Dunning, J., Thom H. Gaussian basis sets for use in correlated molecular calculations. I. The atoms boron through neon and hydrogen. *The Journal of Chemical Physics* **1989**, *90*, 1007–1023.

(59) Kendall, R. A.; Dunning, J., Thom H.; Harrison, R. J. Electron affinities of the firstâ€row atoms revisited. Systematic basis sets and wave functions. *The Journal of Chemical Physics* **1992**, *96*, 6796–6806.

(60) Woon, D. E.; Dunning, J., Thom H. Gaussian basis sets for use in correlated molecular calculations. III. The atoms aluminum through argon. *The Journal of Chemical Physics* **1993**, *98*, 1358–1371.

(61) Groom, C. R.; Bruno, I. J.; Lightfoot, M. P.; Ward, S. C. The Cambridge Structural Database. *Acta Crystallographica Section B* **2016**, *72*, 171–179.

(62) Spek, A. L. Single-crystal structure validation with the program *PLATON*. *Journal of Applied Crystallography* **2003**, *36*, 7–13.

(63) Chisholm, J. A.; Motherwell, S. COMPACK: a program for identifying crystal structure similarity using distances. *Journal of Applied Crystallography* **2005**, *38*, 228–231.

(64) Allen, F. H. The Cambridge Structural Database: a quarter of a million crystal structures and rising. *Acta Crystallographica Section B* **2002**, *58*, 380–388.

(65) Kresse, G.; Furthmüller, J. Efficient iterative schemes for ab initio total-energy calculations using a plane-wave basis set. *Phys. Rev. B* **1996**, *54*, 11169–11186.

(66) Kresse, G.; Furthmüller, J. Efficiency of ab-initio total energy calculations for metals and semiconductors using a plane-wave basis set. *Computational Materials Science* **1996**, *6*, 15–50.

(67) Taylor, C. R.; Day, G. M. Evaluating the Energetic Driving Force for Cocrystal Formation. *Crystal Growth & Design* **2018**, *18*, 892–904.

(68) Grimme, S.; Ehrlich, S.; Goerigk, L. Effect of the damping function in dispersion corrected density functional theory. *Journal of Computational Chemistry* **2011**, *32*, 1456–1465.

(69) Kresse, G.; Joubert, D. From ultrasoft pseudopotentials to the projector augmented-wave method. *Phys. Rev. B* **1999**, *59*, 1758–1775.

(70) Nunez Avila, A. G.; Deschênes-Simard, B.; Arnold, J. E.; Morency, M.; Chartrand, D.; Maris, T.; Berger, G.; Day, G. M.; Hanessian, S.; Wuest, J. D. Surprising Chemistry of 6-Azidotetrazolo[5,1-a]phthalazine: What a Purported Natural Product Reveals about the Polymorphism of Explosives. *The Journal of Organic Chemistry* **2022**, *87*, 6680–6694.

(71) Stone, A.; Alderton, M. Distributed multipole analysis. *Molecular Physics* **1985**, *56*, 1047–1064.

(72) Day, G. M.; Motherwell, W. D. S.; Jones, W. Beyond the Isotropic Atom Model in Crystal Structure Prediction of Rigid Molecules: Atomic Multipoles versus Point Charges. *Crystal Growth & Design* **2005**, *5*, 1023–1033.

(73) Nyman, J.; Day, G. M. Static and lattice vibrational energy differences between polymorphs. *CrystEngComm* **2015**, *17*, 5154–5165.

(74) Widdowson, D.; Kurlin, V. Pointwise distance distributions of periodic sets. *CoRR* **2021**, *abs/2108.04798*.

(75) LeBlanc, L. M.; Dale, S. G.; Taylor, C. R.; Becke, A. D.; Day, G. M.; Johnson, E. R. Pervasive Delocalisation Error Causes Spurious Proton Transfer in Organic Acid–Base Co-Crystals. *Angewandte Chemie International Edition* **2018**, *57*, 14906–14910.

(76) Arlin, J.-B.; Price, L. S.; Price, S. L.; Florence, A. J. A strategy for producing predicted polymorphs: catemeric carbamazepine form V. *Chem. Commun.* **2011**, *47*, 7074–7076.

For Table of Contents Use Only,

Crystal Structure Prediction of Energetic Materials,

Joseph E. Arnold and Graeme M. Day

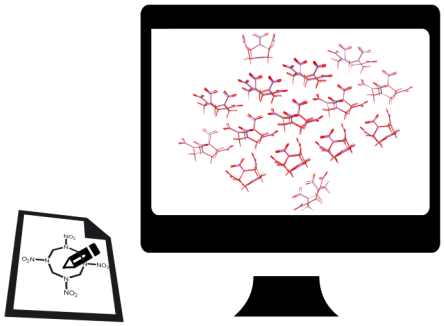

synopsis: The performance of crystal structure prediction methods is assessed on a set of ten molecular organic energetic materials, demonstrating that these methods are sufficiently reliable to be used for the design of new energetic materials.